Bioconjugate Chemistry

Communication

pubs.acs.org/bc

Nanostar Clustering Improves the Sensitivity of Plasmonic Assays

Yong Il Park,[†] Hyungsoon Im,[†] Ralph Weissleder,*[,†,‡] and Hakho Lee*[,†]

[†]Center for Systems Biology, Massachusetts General Hospital, Harvard Medical School, Boston, Massachusetts 02114, United States

[‡]Department of Systems Biology, Harvard Medical School, Boston, Massachusetts 02115, United States

Supporting Information

ABSTRACT: Star-shaped Au nanoparticles (Au nanostars, AuNS) have been developed to improve the plasmonic sensitivity, but their application has largely been limited to single-particle probes. We herein describe a AuNS clustering assay based on nanoscale self-assembly of multiple AuNS and which further increases detection sensitivity. We show that each cluster contains multiple nanogaps to concentrate electric fields, thereby amplifying the signal via plasmon coupling. Numerical simulation indicated that AuNS clusters assume up to 460-fold higher field density than Au nanosphere clusters of similar mass. The results were validated in model assays of protein biomarker detection. The AuNS clustering assay showed higher sensitivity than Au nanosphere. Minimizing the size of affinity ligand was found important to tightly confine electric fields and improve the sensitivity. The resulting assay is simple and fast and can be readily applied to point-of-care molecular detection schemes.

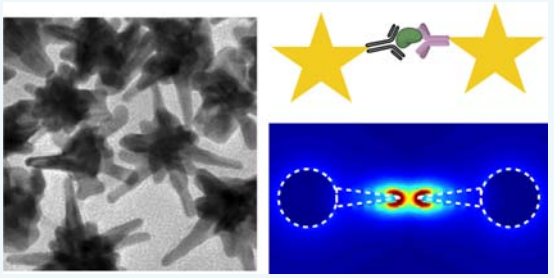

Localized surface plasmon resonance (LSPR) is a promising biosensing strategy for molecular detection.[1−4] Based on surface plasmons that are tightly confined on metallic nanoparticles, LSPR is highly sensitive to changes in dielectric environment surrounding the particles. This unique property has been exploited to detect molecular targets upon their binding to a nanoparticle surface.[5−8]

The most widely used LSPR materials are noble metal (Ag, Au) nanospheres; their synthetic methods are well established, and these particles show plasmon resonance in visible wavelengths.[9] Recently, star-shaped nanoparticles (nanostars) have been explored as an alternative substate to improve the LSPR sensitivity. Nanostars have multiple branches with sharp tips that generate more localized electromagnetic fields than do spherical nanoparticles and thereby produce larger spectral changes upon molecular binding.[10−18] Indeed, Au nanostars have shown >5-fold higher sensitivity than Au nanospheres in LSPR sensing.[19,20] Most previous studies, however, used nanostars as single-particle LSPR probes.[10,13] Namely, the analytical signal was generated when individual nanostars were labeled with target molecules. We hypothesized that the plasmonic signal could be further amplified by inducing the formation of nanostar clusters. This configuration would create multiple nanogaps between nanostars, where electric fields are concentrated and plasmons are coupled.

We herein report on the development and the optimization of such a clustering assay. Using Au nanostars (AuNS) as a substrate, we designed an assay wherein target molecules assemble AuNS into nanoscale-clusters with nanogap junctions. Small AuNS (70 nm in size) with a thiolated ligand were found optimal for sensitive and stable plasmonic sensing. Numerical simulation (finite-difference time-domain/FDTD) showed that a cluster of AuNS can concentrate up to 460-fold higher energy density than an Au nanosphere cluster. We then experimentally verified the results using different molecular interactions (i.e., biotin−avidin and antigen−antibody). The AuNS clustering assay produced much larger spectral shifts than AuNS-ligand alone. Notably, the signal improvement inversely depended on the interparticle distance, which highlighted the importance of minimizing the size of the capturing ligand. The developed assay benefits from fast binding kinetics (<30 min) and a simple signal readout (colorimetry) and could be a potential tool for point-of-care molecular detection.

To synthesize AuNS, we adopted a seed-mediated growth method (see Experimental Procedures in the Supporting Information). Spherical Au nanoparticles (AuNP) with a mean diameter of 13 nm were prepared as a seed (Figure 1a, left) and dispersed in an Au precursor ($HAuCl_4$) solution. Star-shaped Au nanoparticles with multiple branches were formed when ascorbic acid and silver nitrate were injected into the seed solution (Figure 1a, right). The reaction was rapid (<1 min for completion) and produced AuNS with size variations of <30% (Figure S1). We further controlled the overall size of AuNS by changing the molar concentration ratio between Au^{3+} and AuNP seeds ($[Au^{3+}]/[AuNP]$). Higher $[Au^{3+}]/[AuNP]$ ratios led to the synthesis of larger AuNS (Figures 1b and S2). When the ratio was $>2 \times 10^7$, Au precursors spontaneously nucleated, resulting in a mixed phase of AuNP and AuNS (Figure S2). Larger AuNS exhibited a LSPR peak at longer wavelength (Figure 1c and d), because they support more extended longitudinal plasmon resonance along their branches.[21] The peak width also broadened with the particle size (Figure S3),

Received: June 17, 2015
Revised: June 23, 2015
Published: June 23, 2015

DOI: 10.1021/acs.bioconjchem.5b00343
Bioconjugate Chem. 2015, 26, 1470−1474

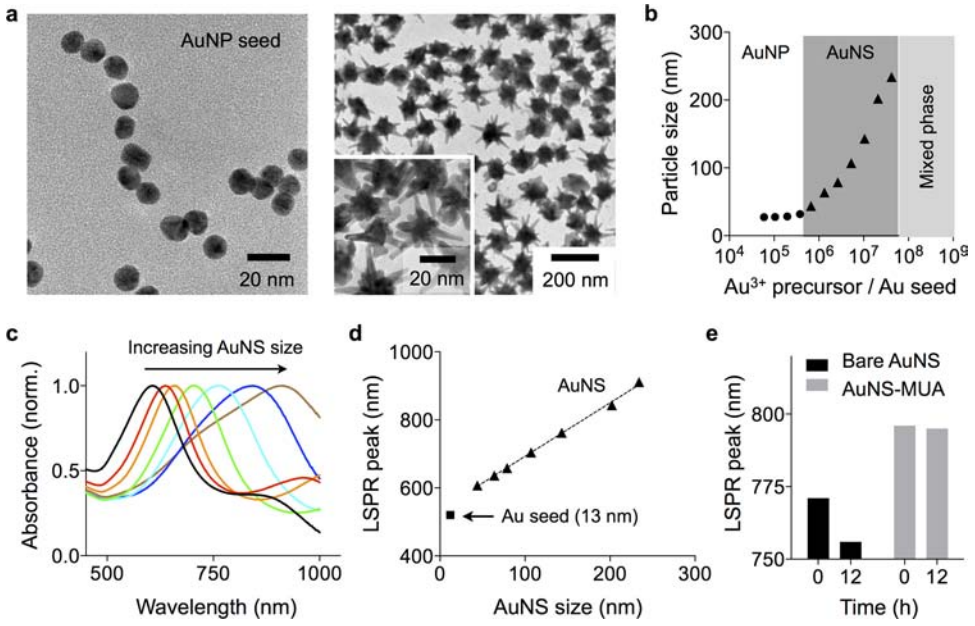

Figure 1. Synthesis and characterization of AuNS. (a) Transmission electron microscopy (TEM) images of AuNP and AuNS. Spherical particles (diameter 13 nm, left) were used as a seed to grow AuNS (right). (b) The size of AuNS was controlled by changing the ratio between AuNP seed and Au^{3+} precursor concentrations. (c, d) Absorbance spectra of AuNS. Increasing the particle size led to shifts of the LSPR peaks to longer wavelengths. (e) Bare AuNS showed a drift in LSPR peak over time. Passivating the AuNS with a thiol ligand (11-mercaptoundecanoic acid/MUA) stabilized the LSPR spectra.

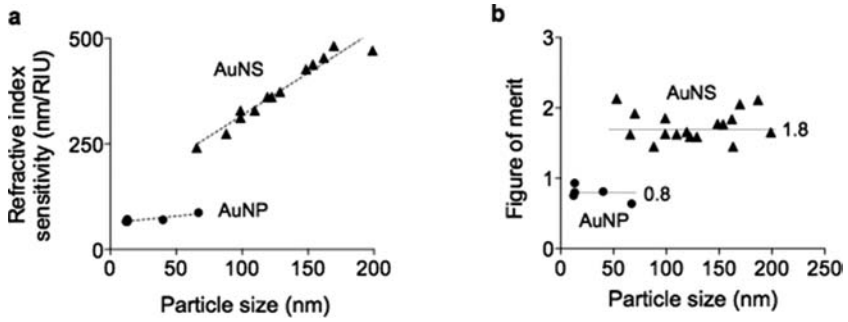

Figure 2. Detection sensitivities of AuNP and AuNS. (a) The refractive index sensitivity (RIS) of AuNS and AuNP of different sizes was measured. The RIS linearly increased with the overall size of the particles. (b) The figure of merit (FOM) was obtained by dividing the RIS with the corresponding full width at half-maximum of the LSPR peak. AuNS assumed higher FOM than AuNP. For a given particle type (i.e., AuNS or AuNP), the FOM values were found similar, independent of the particle size (P = 0.87, AuNS; P = 0.18, AuNP).

which was likely due to the increasing polydispersity (different branch length and number of branches per particle).

As-synthesized bare AuNS were found spectrally unstable; the sharp tips with high surface energy were susceptible to atomic reorganization, which resulted in the shift of the LSPR peaks to shorter wavelengths (Figure 1e).[22−24] We reasoned that thiol-based ligands could stabilize AuNP by forming a covalent bond with surface Au atoms. Indeed, when AuNS were coated with thiol ligands (e.g., lipoic acid, 11-mercaptoundecanoic acid/MUA, thiolated-polyethylene glycol/PEG), the particles maintained their LSPR peak positions (>12 h in phosphate-buffered saline) (Figures 1e and S4).

We next characterized the LSPR properties of individual AuNS. The refractive index sensitivity (RIS) was determined by measuring spectral shifts of particles suspended in solutions of different refractive indices. Water and dimethyl sulfoxide were mixed at varying volume ratios to control the refractive index (see Experimental Procedures in the Supporting Information). The measured RIS of AuNS increased with the overall particle size, ranging from 250 to 500 nm/RIU (refractive index unit, Figure 2a). With similar particle volume, AuNS showed higher RIS than AuNP, validating the advantage of forming sharp branches. For example, the sensitivity of 66 nm AuNS (241 nm/RIU) was 3-fold higher than that of 40 nm spherical AuNP (70 nm/RIU). We also compared the figure of merit (FOM) of particles, that was defined as RIS divided by the full width at half-maximum of the LSPR peak (Figure 2b). Particles with high FOM are preferred as they improve the LSPR detection sensitivity.[7,25] Overall, AuNS had higher FOM (∼1.8) than spherical AuNP (∼0.8). For a given shape, however, the FOM remained similar (coefficient of variation <12%), because both the RIS and peak-width increased with the particle size. For clustering assays, we thus used small AuNS (∼70 nm) for their superior colloidal stability, compared to larger particles.

For molecular sensing with AuNS, we adopted a clustering assay format: AuNS coated with affinity ligands self-assemble into nanoscale clusters in the presence of target molecules (Figure 3a). Such clustering could produce strong plasmonic

DOI: 10.1021/acs.bioconjchem.5b00343
Bioconjugate Chem. 2015, 26, 1470−1474

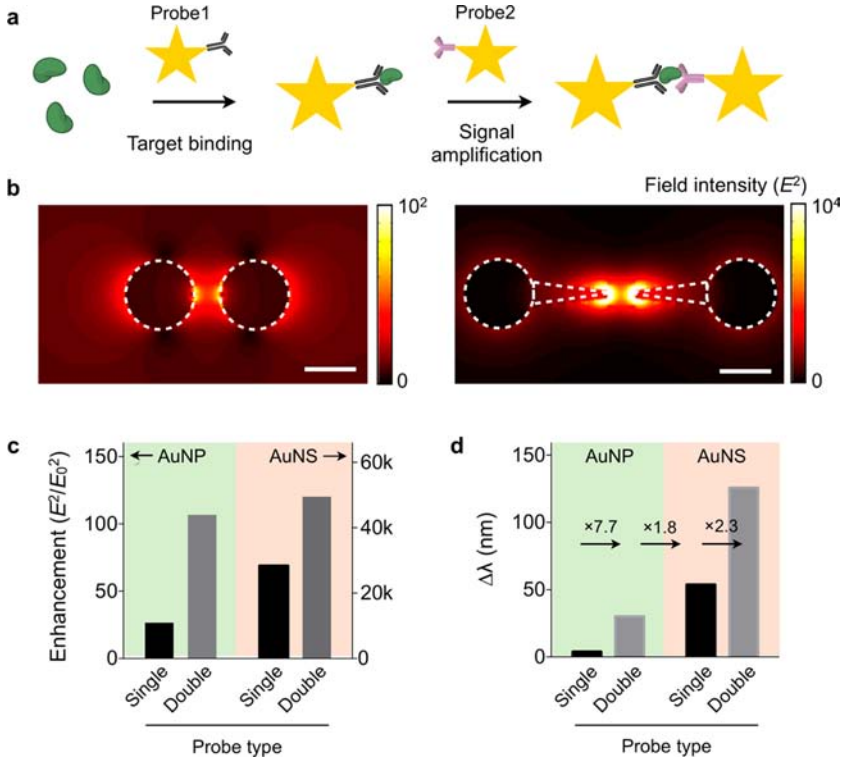

Figure 3. Electromagnetic simulation of the clustering assay. (a) Schematic of the AuNS clustering assay. The target molecule bridges the metal tips of AuNS probes to concentrate electrical fields. (b) Simulated electric field intensity (E^2) surrounding a particle pair. The field magnitude is 460 times higher in the AuNS dimer (right) than in the AuNP dimer (left). Scale bar, 50 nm. (c) The field intensity (E^2) relative to that of the incident light (E_0^2) was compared for different assay configurations. The clustering assay amplifies the signal from the single-probe assay. (d) The spectral shift ($\Delta\lambda$) for each assay type was calculated from the E-field data. The overall sensitivity improved by >32 fold with the AuNS-clustering assay.

coupling among AuNS to increase the spectral shift. We first performed a three-dimensional finite-difference time-domain (FDTD) simulation (Figure S5). We calculated the electric-field (*E*-field) of AuNP and AuNS dimers, a simplified version of clusters. The map showed the field intensity (E^2) concentrated at the junction of two metal particles (Figure 3b). The AuNS dimer showed up to 460-fold higher enhancement than the AuNP dimer (Figure 3c), with *E*-field more efficiently concentrated between tips. The maximum enhancement was observed when two tips of AuNS aligned in a line. Even with misaligned tips, however, the AuNP dimer still showed higher field intensity than the AuNP dimer (Figure S5). The simulation also confirmed that signal amplification could be achieved though particle clustering. Forming a particle-dimer increased the field intensity by 1.7-fold for AuNS (4-fold for AuNP; Figure 3c). Such increases resulted in larger spectral shift ($\Delta\lambda$). The $\Delta\lambda$ for the AuNS dimer, as estimated from the field information, was 2.3-fold larger than AuNS single particle (Figure 3d).

We applied the AuNS clustering assay to detect protein targets. As a model system, we used avidin−biotin interaction and first compared the detection sensitivity between AuNS and AuNP. Biotinylated particles with similar volumes (AuNP, 40 nm in diameter; AuNS, 70 nm in overall size) were prepared and concentration-matched (see Experimental Procedures in the Supporting Information for details). Varying concentrations of avidin were added to particle solutions, and resulting spectral shifts ($\Delta\lambda$) were measured. In the presence of avidin, the particles clustered and their spectral peaks red-shifted (Figure 4a). Dynamic light scattering measurements confirmed the avidin-specific clustering; the hydrodynamic diameter increased with avidin concentration (Figure S6). Dark-field microscopy could also detect AuNS clustering.[26] The aggregated particles appeared brighter than individual particles due to the increased scattering cross-section (Figure S7).[26] The microscopy, however, has a limited assay speed and throughput and requires fine-tuning of particle concentrations to obtain optimal particle numbers in a field-of-view. In all concentrations tested, AuNS showed larger $\Delta\lambda$ than AuNP. For instance, with the addition of 16 nM of avidin, $\Delta\lambda$ = 19 nm for AuNS, and $\Delta\lambda$ = 1.5 nm for AuNP. Titration measurements further confirmed the superiority of AuNS over AuNP (Figure 4b), with AuNS displaying a 7-fold lower limit of detection (LOD = 3.4 nM) than AuNP (LOD = 23.4 nM).

We next examined the effect of the interparticle distance on the clustering assay sensing. Reducing the interparticle distance (d_{pp}) is crucial in improving the detection sensitivity, since the field enhancement between the tips decreases exponentially with d_{pp} (Figure S8). As a model detection target, we used the kidney injury molecule-1 (KIM1), a urinary protein marker for kidney injury.[27] To control the particle distance, we prepared two types of probes (see Experimental Procedures in the Supporting Information): AuNS conjugated with full polyclonal antibodies (Ab-AuNS) and AuNS with half antibody fragments ($Ab_{1/2}$-AuNS). As a control, we prepared AuNS conjugated with isotype-matched IgG antibodies. The KIM1 titration experiments showed dose-dependent spectral shifts (Figure 4c), with the half antibody configuration displaying larger spectral shifts than that with the full-antibody probes. When BSA was used as a control analyte, we observed negligible signal changes (Figure S9); this confirmed that the signal changes were due to antibody−antigen specific aggregation. The LOD for $Ab_{1/2}$-

DOI: 10.1021/acs.bioconjchem.5b00343
Bioconjugate Chem. 2015, 26, 1470−1474

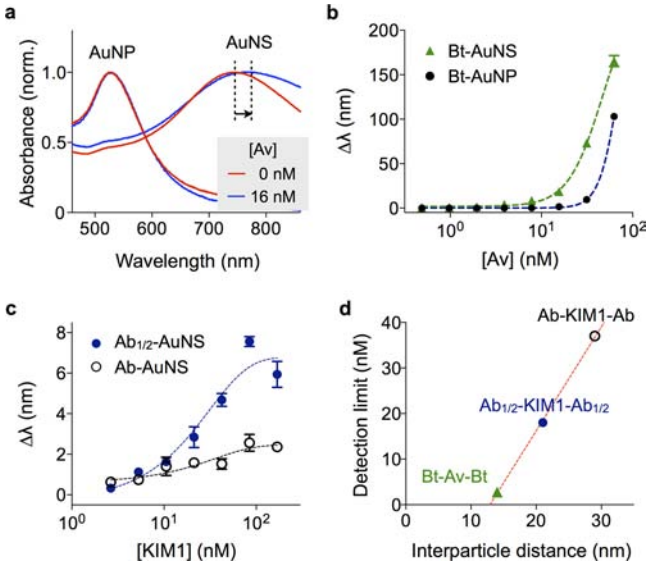

Figure 4. Protein detection with AuNS. (a) Biotinylated AuNP (Bt-AuNP) and AuNS (Bt-AuNS) with similar particle volumes were incubated with avidin, and the corresponding spectral changes were monitored. With the addition of 16 nM of avidin, Bt-AuNS displayed more pronounced spectral shifts ($\Delta\lambda$ = 19 nm) than Bt-AuNP ($\Delta\lambda$ = 1.5 nm). (b) Avidin-titration experiments confirmed the superior sensitivity of the AuNS system. The limit of detection (LOD) of Bt-AuNS was 7 times lower than that of Bt-AuNP. (c) The effect of the interparticle distance on the assay sensitivity was studied. Kidney injury molecule-1 (KIM1) was used as the detection target. To change the interparticle distance, AuNS was conjugated with either full antibody against KIM1 (Ab-AuNS) or half antibody fragments ($Ab_{1/2}$-AuNS). The shorter probe ($Ab_{1/2}$-AuNS) produced larger LSPR spectral shifts in KIM1 titration measurements. AuNS conjugated with isotype-matched goat IgG was used as control. (d) The detection limits of the three systems in (b) and (c) were compared. The detection sensitivity was found to be inversely proportional to the interparticle distance.

AuNS was 2-fold lower than that of Ab-AuNS. We further compared the detection sensitivity as a function of the interparticle distance (Figure 4d, Table S1). The LOD values were obtained from the titration experiments (Figure 4b and 4c), and d_{pp} was estimated from the lengths of the passivation layer, affinity ligands, and target molecules. The avidin−biotin system ($d_{pp} \approx 12$ nm) showed the lowest detection limit (the highest sensitivity), followed by the half antibody−antigen ($d_{pp} \approx 19$ nm) and the full-antibody−antigen ($d_{pp} \approx 33$ nm) systems. The improved sensitivity (2-fold) with a shorter interparticle distance is consistent with our numerical simulation data (Figure S8).

In summary, AuNS are promising nanoprobes for plasmonic biosensing. With multiple branched tips at their surface, AuNS can concentrate electromagnetic fields more efficiently compared to spherical particles and thereby generate larger plasmonic spectral shifts upon molecular binding. In this study, we found three key aspects to improve sensitive biosensing with AuNS, namely 1) a covalent surface coating to maintain particle morphology and its resonance spectra; 2) AuNS clustering to more strongly concentrate electromagnetic energy; and 3) minimizing the interparticle distance in AuNS clusters. The resulting AuNS assay was simple and fast, as the reaction occurs in bulk solution and the signals can be read out from visual color changes. Compared to the microscopic observation of individual AuNS, the method is also scalable for high throughput detection. We envision that this assay could have potential applications in point-of-care molecular detection.

■ ASSOCIATED CONTENT

Supporting Information

Experimental procedures, Figures S1−S9, and Table S1. The Supporting Information is available free of charge on the ACS Publications website at DOI: 10.1021/acs.bioconjchem.5b00343.

■ AUTHOR INFORMATION

Corresponding Authors

*Phone: 617-726-8226. E-mail: rweissleder@mgh.harvard.edu. Corresponding author address: Center for Systems Biology, Massachusetts General Hospital, 185 Cambridge St, CPZN 5206, Boston, MA 02114 (R.W.).

*E-mail: hlee@mgh.harvard.edu. Corresponding author address: Center for Systems Biology, Massachusetts General Hospital, 185 Cambridge St, CPZN 5206, Boston, MA 02114 (H.L.).

Notes

The authors declare no competing financial interest.

■ ACKNOWLEDGMENTS

We thank K. Lee for microscopy imaging and H. Shao and H. J. Chung for helpful discussions. This work was supported in part by NIH Grants R01HL113156, R01EB004626, R01EB010011, HHSN268201000044C, U54-CA119349, and T32-CA79443 and Department of Defense OCRP Program Award W81XWH-14-1-0279.

■ REFERENCES

(1) Hutter, E., and Fendler, J. H. (2004) Exploitation of localized surface plasmon resonance. *Adv. Mater. 16*, 1685−1706.

(2) Anker, J. N., Hall, W. P., Lyandres, O., Shah, N. C., Zhao, J., and Van Duyne, R. P. (2008) Biosensing with plasmonic nanosensors. *Nat. Mater. 7*, 442−453.

(3) Jain, P. K., Huang, X., El-Sayed, I. H., and El-Sayed, M. A. (2008) Noble metals on the nanoscale: optical and photothermal properties and some applications in imaging, sensing, biology, and medicine. *Acc. Chem. Res. 41*, 1578−1586.

(4) Sepulveda, B., Angelome, P. C., Lechuga, L. M., and Liz-Marzan, L. M. (2009) LSPR-based nanobiosensors. *Nano Today 4*, 244−251.

(5) Haes, A. J., and Van Duyne, R. P. (2002) A nanoscale optical blosensor: Sensitivity and selectivity of an approach based on the localized surface plasmon resonance spectroscopy of triangular silver nanoparticles. *J. Am. Chem. Soc. 124*, 10596−10604.

(6) Sherry, L. J., Jin, R., Mirkin, C. A., Schatz, G. C., and Van Duyne, R. P. (2006) Localized surface plasmon resonance spectroscopy of single silver triangular nanoprisms. *Nano Lett. 6*, 2060−2065.

(7) Mayer, K. M., and Hafner, J. H. (2011) Localized surface plasmon resonance sensors. *Chem. Rev. 111*, 3828−3857.

(8) Gao, B., Rozin, M. J., and Tao, A. R. (2013) Plasmonic nanocomposites: polymer-guided strategies for assembling metal nanoparticles. *Nanoscale 5*, 5677−5691.

(9) Lu, X., Rycenga, M., Skrabalak, S. E., Wiley, B., and Xia, Y. (2009) Chemical synthesis of novel plasmonic nanoparticles. *Annu. Rev. Phys. Chem. 60*, 167−192.

(10) Nehl, C. L., Liao, H., and Hafner, J. H. (2006) Optical properties of star-shaped gold nanoparticles. *Nano Lett. 6*, 683−688.

(11) Hao, F., Nehl, C. L., Hafner, J. H., and Nordlander, P. (2007) Plasmon resonances of a gold nanostar. *Nano Lett. 7*, 729−732.

(12) Senthil, K., Pandian, Pastoriza-Santos, I., Rodriguez-Gonzalez, B., Garcia, d. A., Javier, F., and Liz-Marzan, L. M. (2008) High-yield

DOI: 10.1021/acs.bioconjchem.5b00343
Bioconjugate Chem. 2015, 26, 1470−1474

synthesis and optical response of gold nanostars. *Nanotechnology 19*, 015606.
(13) Dondapati, S. K., Sau, T. K., Hrelescu, C., Klar, T. A., Stefani, F. D., and Feldmann, J. (2010) Label-free biosensing based on single gold nanostars as plasmonic transducers. *ACS Nano 4*, 6318−6322.
(14) Barbosa, S., Agrawal, A., Rodriguez-Lorenzo, L., Pastoriza-Santos, I., Alvarez-Puebla, R. A., Kornowski, A., Weller, H., and Liz-Marzan, L. M. (2010) Tuning size and sensing properties in colloidal gold nanostars. *Langmuir 26*, 14943−14950.
(15) Guerrero-Martinez, A., Barbosa, S., Pastoriza-Santos, I., and Liz-Marzan, L. M. (2011) Nanostars shine bright for you Colloidal synthesis, properties and applications of branched metallic nanoparticles. *Curr. Opin. Colloid Interface Sci. 16*, 118−127.
(16) Vo-Dinh, T., Fales, A. M., Griffin, G. D., Khoury, C. G., Liu, Y., Ngo, H., Norton, S. J., Register, J. K., Wang, H. N., and Yuan, H. (2013) Plasmonic nanoprobes: from chemical sensing to medical diagnostics and therapy. *Nanoscale 5*, 10127−10140.
(17) Webb, J. A., Erwin, W. R., Zarick, H. F., Aufrecht, J., Manning, H. W., Lang, M. J., Pint, C. L., and Bardhan, R. (2014) Geometry-Dependent Plasmonic Tunability and Photothermal Characteristics of Multibranched Gold Nanoantennas. *J. Phys. Chem. C 118*, 3696−3707.
(18) Solis, D. M., Taboada, J. M., Obelleiro, F., Liz-Marzan, L. M., and Garcia de Abajo, F. J. (2014) Toward ultimate nanoplasmonics modeling. *ACS Nano 8*, 7559−7570.
(19) Lu, W., Singh, A. K., Khan, S. A., Senapati, D., Yu, H., and Ray, P. C. (2010) Gold nano-popcorn-based targeted diagnosis, nanotherapy treatment, and in situ monitoring of photothermal therapy response of prostate cancer cells using surface-enhanced Raman spectroscopy. *J. Am. Chem. Soc. 132*, 18103−18114.
(20) Yuan, H., Liu, Y., Fales, A. M., Li, Y. L., Liu, J., and Vo-Dinh, T. (2013) Quantitative surface-enhanced resonant Raman scattering multiplexing of biocompatible gold nanostars for in vitro and ex vivo detection. *Anal. Chem. 85*, 208−212.
(21) Khoury, C. G., and Vo-Dinh, T. (2008) Gold Nanostars For Surface-Enhanced Raman Scattering: Synthesis, Characterization and Optimization. *J. Phys. Chem. C 2008*, 18849−18859.
(22) Im, H., and Oh, S. H. (2014) Oxidation sharpening, template stripping, and passivation of ultra-sharp metallic pyramids and wedges. *Small 10*, 680−684.
(23) Malinsky, M. D., Kelly, K. L., Schatz, G. C., and Van Duyne, R. P. (2001) Chain length dependence and sensing capabilities of the localized surface plasmon resonance of silver nanoparticles chemically modified with alkanethiol self-assembled monolayers. *J. Am. Chem. Soc. 123*, 1471−1482.
(24) Vega, M. M., Bonifacio, A., Lughi, V., Marsi, S., Carrato, S., and Sergo, V. (2014) Long-term stability of surfactant-free gold nanostars. *J. Nanopart. Res. 16*, 2729.
(25) Joshi, G. K., McClory, P. J., Muhoberac, B. B., Kumbhar, A., Smith, K. A., and Sardar, R. (2012) Designing Efficient Localized Surface Plasmon Resonance-Based Sensing Platforms: Optimization of Sensor Response by Controlling the Edge Length of Gold Nanoprisms. *J. Phys. Chem. C 116*, 20990−21000.
(26) Bu, T., Zako, T., Fujita, M., and Maeda, M. (2013) Detection of DNA induced gold nanoparticle aggregation with dark field imaging. *Chem. Commun. 49*, 7531−7533.
(27) Waanders, F., van Timmeren, M. M., Stegeman, C. A., Bakker, S. J., and van Goor, H. (2010) Kidney injury molecule-1 in renal disease. *J. Pathol. 220*, 7−16.

DOI: 10.1021/acs.bioconjchem.5b00343
Bioconjugate Chem. 2015, 26, 1470−1474